Published in final edited form as:
Cancer Biol Ther. 2009 October ; 8(20): 1940–1946.

Atrasentan (ABT-627) enhances perfusion and reduces hypoxia in a human tumor xenograft model

Kwang Mo Yang[1,2,†], **James Russell**[1,*,†], **Mihaela E. Lupu**[1], **HyungJoon Cho**[1], **Xiao-Feng Li**[1,3], **Jason A. Koutcher**[1], and **C. Clifton Ling**[1]

[1]Department of Medical Physics; Memorial Sloan-Kettering Cancer Center; New York, NY USA

[2]Korean Institute of Radiological & Medical Sciences; Nowon-Gu, Seoul Korea

[3]Department of Diagnostic Radiology; University of Louisville School of Medicine; Louisville, KY USA

Abstract

The endothelin-1 antagonist, Atrasentan (ABT-627) was used to modify perfusion in the human tumor xenograft model, HT29, growing in nude mice. Atrasentan produced a significant increase in perfusion, as measured in vivo by Gd-DTPA DCE-MRI. Changes in tumor hypoxia were assessed by comparing the binding of two hypoxia tracers, pimonidazole and EF5 given before and after Atrasentan administration. In vehicle-treated controls, the distribution of EF5 and pimonidazole was very similar. However, Atrasentan treatment was associated with decreased uptake of the second hypoxia tracer (EF5), relative to the first (pimonidazole). Although Atrasentan had no independent effect on the growth of HT29 tumors, Atrasentan combined with 20 Gy radiation led to a modest but significant increase in tumor growth delay compared to radiation alone.

Keywords

Atrasentan; tumor hypoxia; tumor perfusion; HT29; pimonidazole; EF5

Introduction

The endothelins (ET-1, ET-2 and ET-3) are 21 amino acid peptides involved primarily in controlling vascular tone. ET1, the most common, is a potent vasoconstrictor that acts through binding to the cell surface receptors ET_A and ET_B.[1] ET_A and ET_B receptors antagonize each other; ET_A receptors induce vasoconstriction, while ET_B receptors induce vasodilation. All three endothelins can bind equally to ET_B, but only ET-1 and ET-2 can bind ET_A.[2] ET_A receptors are expressed in vascular smooth muscle cells, where ET-1 binding induces vasoconstriction. ET_A receptors are also present on a variety of other normal tissues,[3–5] and in cancer cells,[6–10] where receptor binding suppresses paclitaxel-induced apoptosis[11–14] and induces mitogenesis.[8,15,16] Multiple ET_A antagonists have been advanced into clinical trials, to treat both cancer[17–19] and vascular pathologies, principally pulmonary arterial hypertension.[20]

While oncologists have mostly been interested in the cytotoxicity of inhibiting ET_A in tumor cells, recent results from Martinive et al. suggest that the vasodilatory effects of ET_A inhibition

*Correspondence to: James Russell; russellj@mskcc.org.
†These authors contributed equally to this work.

could increase tumor perfusion, thus enhancing drug delivery[21] and reducing tumor hypoxia.[22] In vitro, hypoxia has long been known to significantly reduce the cytotoxic effects of ionizing radiation, and reducing tumor hypoxia in the clinic improves the response to radiotherapy.[23] Thus ET_A blockade offers three advantages in cancer therapy: increased drug supply to the tumor; increased sensitivity to the drug; and increased sensitivity to radiation via better oxygenation. In some radiotherapy protocols, nicotinamide is used to increase perfusion.[24] However, nicotinamide does not seem to be effective in every tumor[25] and an alternative treatment would be valuable.

The Martinive studies achieved ET_A inhibition by the peptide BQ123.[21] However BQ123 is not considered a clinically useful agent, partly because of cost issues. Instead pharmaceutical companies have developed a class of agents known as the "sentans," of which five antagonize both the ET_A and ET_B receptors, while ten are specific ET_A antagonists.[20]

One such agent is Atrasentan (ABT-627), which is currently in clinical trials.[17–19] It is highly specific for the ET_A receptor,[26] and has been shown to restrict the growth of cervical cancer xenografts[27] and enhance the effects of taxane therapy in prostate cancer xenografts.[28] Moreover, it has been demonstrated to reduce vasoconstriction in rats[29,30] and mice.[31] In this report, we asked whether, like BQ123, Atrasentan could increase perfusion and reduce hypoxia in an experimental tumor model.

Hypoxic tissue can be detected through immunohistochemistry using the 2-nitro-imidazole compounds pimonidazole and EF5. Both agents are subject to enzyme-mediated reduction, followed by covalent binding to macromolecules, and the bound adducts can be recognized by antibodies. The process is inhibited in the presence of oxygen. Both pimonidazole and EF5 have been used clinically to determine tumor hypoxia.[32,33] By administering nitroimidazole markers separately, it is possible to determine changes in tumor hypoxia in the interval between tracer injections, a technique pioneered by Ljungkvist et al.[34]

Results

Effect of atrasentan on tumor perfusion

To test whether Atrasentan enhanced tumor perfusion, seven tumor bearing mice were subjected to Gd DTPA DCE MRI. MRI was performed immediately before Atrasentan injection, and repeated six h later. Ak_{ep} maps of a representative tumor are shown in Figure 1. Areas of highest perfusion are represented in red; areas of lowest perfusion are represented in blue. Figure 1A shows representative MR slices before treatment; Figure 1B shows maps from the same tumor after the treatment. For six out of seven tumors, the median Ak_{ep} values increased in the post-treatment scan (Fig. 1C). Overall there was a significant increase in the median Ak_{ep} values after treatment; significance was judged by a two-tailed paired t-test ($p = 0.032$). Atrasentan treatment approximately doubled tumor Ak_{ep} values: the mean ratio of Ak_{ep}s post-treatment relative to pre-treatment was 1.95, with 95% confidence intervals of 1.4–2.5.

Effect of atrasentan on tumor hypoxia

To determine whether increased perfusion would lead to decreased tumor hypoxia, tumor bearing mice were injected with the hypoxia markers pimonidazole and EF5, separated by 24 h. In HT29 tumors we have previously shown that pimonidazole and EF5 yield identical staining patterns when co-injected. We have also shown in this model that tumor hypoxia changes spontaneously over 24 hours, with the appearance of both newly hypoxic and newly oxygenated tissue. However, this effect is very limited in scale; it was not sufficient to prevent the observation of carbogen-induced changes in hypoxia and would not be expected to prevent

observation of drug-induced changes in hypoxia.[35] We have also shown that this protocol is efficient at detecting artificially induced changes in hypoxia in the HT29 system. A total of four control and five treated mice were used. Figure 2A and B show images of a control tumor stained for pimonidazole and EF5 respectively. The control tumors show good agreement between pimonidazole and EF5—i.e., the staining patterns are remarkably similar. As seen in Figure 2C and D, Atrasentan treatment clearly reduces EF5 (Fig. 2D) uptake relative to pimonidazole (Fig. 2C). Subjectively, it seems to be the case that EF5 uptake is least affected in peri-necrotic tissue. For the tumor in Figure 2C and D, pre-treatment hypoxia is found both adjacent to large areas of necrosis, and spread through the tumor in small islands. It was these islands that were most susceptible to Atrasentan treatment. The tumor shown in Figure 3A and B was also treated with Atrasentan. However, the effect of Atrasentan is not detectable, and this may be due to the largely peri-necrotic nature of the hypoxia found in this tumor.

Quantitative analysis of immunohistochemical staining

We quantified the staining in two ways: thresholds were applied to the pimonidazole and EF5 images to derive the fractions of the tumor section that was positive for each marker. The results are shown in Table 1, which was derived by applying a threshold of 70 to all images. Threshold values are inevitably arbitrary, and subject to the possibility that a different threshold value would yield different results. To investigate this possibility, we exported all image histograms into Excel and generated positive fractions for each threshold value. In addition statistical significance was calculated for each threshold value using a two-tailed t-test and assigning significance to all p values <0.05. As shown in Figure 4, a significant difference between treated and control images would be obtained over a wide range of threshold values. The upward curve of the controls seems to indicate a discrepancy between EF5 and pimonidazole staining at high thresholds. However, in the control data set at high threshold values there was a lot of scatter, and the ratio of EF5 to pimonidazole was not significantly different from unity. Moreover, using this analysis technique, we have previously found the EF5 to pimonidazole ratio to closely approximate unity.[35] Thus we do not think that this plot suggests some fundamental difference in the behavior of these two tracers.

Secondly, the red and green values for each pixel in viable tumor tissue were entered into correlation analysis, using software written in-house. Examples of representative dot-plots generated for control and treated tumors are shown in Figure 5A and B, respectively. The slopes of the regression lines were consistently shallower for treated tumors relative to controls—0.98 compared to 0.69, $p = 0.04$.

Effect of atrasentan on tumor response to radiation

We tested whether the reduced hypoxia that we observed by immunohistochemistry would translate into an increased response to radiation. Figure 6 shows the regrowth of tumors after Atrasentan treatment, 20 Gy ionizing radiation, and Atrasentan plus ionizing radiation. Atrasentan itself had no effect on tumor growth. However, there was a modest increase in the median growth delay when Atrasentan was combined with radiation (52.6 vs. 60.3 d). The data was analyzed by a two-tailed Mann-Whitney test; this yielded a p value of 0.046 for radiation versus radiation plus Atrasentan. Figure 6 shows the median tumor volume, as opposed to the more conventional mean. The median was selected as plotting the mean volume inappropriately overstated the difference between radiation and radiation plus Atrasentan.

Discussion

We have shown that Atrasentan increases tumor perfusion as measured by Gd DTPA DCE MRI. There was an approximate doubling of the Ak_{ep} value due to Atrasentan, observable at 6 h after treatment. This time was selected based on work by Opgenorth et al.[36] who showed

that Atrasentan was active in rats over a period of 4–24 h post-dosing. Also Verhaar et al. showed that while Atrasentan could reduce vasoconstriction in humans, the effect was not seen immediately: they attributed this lag to the time needed to displace Endothelin 1 from the ET_A receptor.[37] However, Sonveaux et al. were able to demonstrate changes in perfusion and hypoxia in mice one hour after BQ123 administration, [22] suggesting that Atrasentan would also have been active at earlier time points in mice.

Enhanced perfusion was followed by diminished hypoxia. The ratio of EF5 to pimonidazole represents the fractional change in hypoxia over the course of the experiment, and this ratio was significantly lower in treated tumors compared to controls. The ratio of EF5 to pimonidazole is obtained by applying thresholds to the immunostained images and classifying area of tumor as positive or negative. Statistical significance was largely independent of the threshold setting. However, the magnitude of the effect was not: at a threshold of 70 (Table 1), there was an approximately 50% reduction in EF5/pimonidazole in the treated group. This value would increase or decrease with higher or lower threshold values respectively. Thus it is not possible to precisely quantify the effects of Atrasentan on tumor hypoxia.

In this context it should be noted that hypoxia in the HT29 models appears in two patterns: it can be present in apparently viable tissue, or it can be seen bordering large areas of necrosis. Regions of viable hypoxic tissue are generally small, being typically about 100 microns thick. Atrasentan generally did not reduce hypoxia in peri-necrotic regions, but was effective against hypoxia in fully viable tissue. An example of this is shown in Figures 2 and 3.

When Atrasentan was combined with radiation there was a modest but real effect on tumor regrowth. A dose of 20 Gy has been shown to reduce survival in HT29 tumors to well below 1% of the total;[38] thus this treatment should have effectively sterilized all non-hypoxic cells in the tumor. Regrowth of the tumor should be due to expansion of those cells which were hypoxic at the time of radiation. Atrasentan could only influence tumor response to 20 Gy by acting on the hypoxic cells in some manner. While the regrowth data does not rule out the possibility that Atrasentan radiosensitized the hypoxic population, based on the results discussed above, we consider it more likely that Atrasentan had reduced the size of the hypoxic population.

However, although Atrasentan could clearly reduce tumor hypoxia, we did not in these experiments observe that it had the ability to abolish hypoxia. Subjectively, the immunochemistry images seemed to indicate that Atrasentan was least effective against peri-necrotic hypoxia, and the MRI images also indicated the largest Atrasentan effect was in the tumor periphery. This may reflect a specific limitation of the agent, or it may be that there is a more general limit to vasodilation, since to enhance tumor perfusion there must first be a concentration of unperfused vessels. Our data suggest that Endothelin-1 antagonism deserves further study as a means to reduce tumor hypoxia, particularly in combination with carbogen, which is currently used to augment nicotinamide-induced vasoldilation.[24]

Materials and Methods

Tumor model

The human colorectal carcinoma cell line HT29 was obtained from ATCC (Manassas, VA) and maintained in exponential growth phase in McCoy's 5A modified medium supplemented with 10% fetal calf serum. Xenografts were generated by subcutaneously injecting 5×10^6 tumor cells in 100 μl of PBS in the flank adjacent to the right hind limb of male immune-compromised NCI *nu/nu* mice (~20 g, Frederick Cancer Research Institute, Frederick, MD). Experiments were performed when tumours reached 10–13 mm in diameter. The mice were

maintained and used according to protocols approved by the Institutional Animal Care and Use Committee of Memorial Sloan Kettering Cancer Center.

Animal manipulation

Atrasentan was generously supplied by Abbott Laboratories (Chicago, IL). Atrasentan was dissolved in ethanol at 80 mg/ml, and further diluted in 0.05 N NaOH/saline to 4 mg/ml, pH 12. Atrasentan was prepared prior to each experiment, and injected intraperitoneally at 20 mg/kg, in an injection volume of 0.1 ml. Control animals were injected with vehicle. EF5 (provided by Dr. C.J. Koch), and pimonidazole hydrochloride (Hypoxyprobe-1, HPI, Burlington, MA) were dissolved in PBS and administered via the tail vein at 30, and 120 mg/kg respectively. The injection volumes were 0.2 ml. Pimonidazole and EF5 were injected 24 hours and one hour before sacrifice, respectively. Atrasentan was injected 5 hours before sacrifice.

After the mice were sacrificed, the tumours were removed and frozen in OCT mounting medium (Sakura Finetek, Torrance, CA). Consecutive 10 μm thick sections were cut on a Microm HM500 cryostat microtome (Microm International GmbH, Walldorf, Germany). Each treatment group contained three to four mice.

DCE-MRI

The DCE-MRI experiments were performed on a Bruker 4.7T BioSpin (Bruker, Germany). A syringe filled with the contrast agent Gd-DTPA; 0.1 mmol Gd/kg, (Magnevist®, Berlex Laboratories, Inc., Wayne, NJ) was connected to an INT stopper (B. Braun Medical Inc., Bethlehem, PA) via a Gd-DTPA-filled tubing (Inner Diameter: 0.8 mm, Length: 16 inches, Masterflex Norprene® tubing, 6402-13). Animals were placed prone inside a whole-body bird cage MR coil (diameter, 1.5 inches; length, 5-1/2 inches, Bruker, Germany) with a respiration monitor pad (SA Instruments, Inc., Stonybrook, NY) placed under the abdomen for monitoring during the study. With the help of a horizontal bubble level and the axial MR profile, the tumor was placed in the center of the magnet. The MRI coil was tuned and matched to the proton frequency (200 MHz) inside the magnet, followed by shimming of the sample. The coronal slices of interest were determined from a pilot scan. T_2-weighted MR images (Rapid Acquisition with Refocused Echoes: relaxation time, 2,000 ms; excitation time, 40 ms; number of repeat images, 1; number of averages 8; slice thickness 1 mm; number of slices 2; field of view 2 cm × 2.5 cm, matrix = 160 × 128) were acquired to visualize clearly the boundary between tumor and muscle tissue. T_1-weighted DCE-MRI (Gradient Echo: relaxation time, 50 ms; excitation time, 2.3 ms; number of repeat images, 125; number of averages, 2; slice thickness, 1 mm; number of slices, 2; field of view, 2 cm × 2.5 cm; matrix = 128 × 96; flip angle, 30°) was performed at 9 s temporal resolution. The contrast agent Gd-DTPA was injected via tail vein after 2 minutes of baseline acquisition followed by 20 minutes of dynamic acquisition. After the MRI acquisition, animals were removed from the animal holder, Atrasentan was injected intraperitoneally, and the animals were returned to the cage. The catheter was kept patent by injection of heparinized saline. Six hours after the baseline DCE-MRI experiment, another DCE-MRI experiment was performed to monitor the change in perfusion due to the injection of drug. The animal was re-positioned in the MR coil and was placed in the center of the magnet following the same procedure as used for the baseline DCE-MRI scan. After shimming, T_2-weighted MR images were obtained, followed by T_1-weighted DCE-MRI using the same MR parameters with baseline experiment. The contrast agent Gd-DTPA was also injected via tail vein after 2 minutes of baseline acquisition followed by 20 minutes of dynamic acquisition. After post DCE-MRI scan, animals were removed from the MR coil and sacrificed.

MR time-signal curves from tumor slices before and after treatment were obtained from the T_1-weighted signal intensity of each individual voxel in the dynamic MR images after Gd-

DTPA administration. To obtain these time-signal curves, the reconstructed Bruker MR image files were converted to Analyze format using Micro Bruker2AnlyzeConverter (Bru2Anz, by C. Rorden, Columbia, SC, http://www.sph.sc.edu/comd/rorden/bru2anz.html) software and the MR images in Analyze format were processed with custom-written MatLab (The MathWorks, Inc., Natick, MA) scripts. The experimental time-signal curves for each individual voxel in the MR images were normalized with respect to the baseline signal (averaged over initial 2 minutes of acquisition without the contrast agent) and were fitted using the model developed by Hoffman et al.[39] for each slice. This model is based on the linear relationship between measured saturation recovery MR signal and the concentration of Gd-DTPA in the tissue. An amplitude (A), which reflects the degree of relative MR signal enhancement and an exchange rate (k_{ep}), which characterizes the velocity of MR signal increase can be obtained via pharmacokinetic modeling of the two compartment model. Consequently, the value of Ak_{ep} is analogous to the slope of MR signal enhancement for initial time and is considered an approximate measure of vascular flow/perfusion of the tumor tissue. The Hoffman model was used to estimate Ak_{ep} values of individual voxels from the dynamic build up curves, and Ak_{ep} maps were generated for tumor slices before and after treatment. It has been observed that the majority of tumors have necrotic regions in the core as verified by modest Gd-DTPA uptake in the core of tumors. To quantify the change in the perfusion of tumor due to the treatment excluding the necrotic area, a mask including a 1.5 mm-thick rim of tumor was generated using T_2-weighted images of the corresponding slice. A histogram analysis was performed for both Ak_{ep} values in the rim of tumors before and after treatment. To calculate the median values of Ak_{ep} distribution for each rim of tumor, Ak_{ep} values from two MR slices for each animal were added and one median value was calculated for a corresponding tumor rim before and after treatment. The effect of Atrasentan was assessed by a paired two-tailed t-test; a value of $p < 0.05$ was considered significant.

Immunohistochemical staining

For EF5 and pimonidazole staining, sections were air-dried for 30 min, fixed in icecold methanol for 30 min and incubated in SuperBlock® (Pierce, Rockford, IL) overnight at 4°C. Cy3 conjugated anti-EF5 (supplied by Dr. C.J. Koch) was applied at a concentration of 75 μg/ml for 1 h at room temperature. Slides were washed three times in PBS, and treated with sheep anti-cyanine (25 μg/ml, US Biologicals, Marblehead, MA) in mouse serum/Superblock (1:1) for one hour at room temperature. Slides were washed again and simultaneously exposed to FITC-conjugated anti-pimonidazole (1:20, HPI) and Alexafluor 568 anti-sheep (InVitrogen, Carlsbad CA) at 20 μg/ml in Superblock. Slides were washed three times and imaged on a fluorescent microscope.

Image acquisition and analysis

Images were acquired using a Nikon Diaphot 300 microscope (Nikon Instruments, Melville, NY) equipped with a xenon arc lamp (Sutter Instrument, Novato, CA) and appropriate filters for FITC and TRITC fluorescence (Chroma Technology, Rockland VT). Entire tumor sections were captured by collecting multiple fields using a ×10 objective lens. Individual fields were acquired using a computer-controlled stage motor (LUDL Electronic Products, Hawthorne, NY) and a Coolsnap cooled charge-coupled device digital camera (Photometrics, Tuscon, AZ). Composite images were stitched together using ImagePro software (MediaCybernetics, Silver Spring, MD). Images were saved in 8-bit format for analysis in Adobe Photoshop (Adobe, San Jose, CA).

Necrosis could be easily recognized on the fluorescent images and these areas were excluded from analysis. For each image, the background (off-section) brightness was obtained, and subtracted from the total image. Then regions displaying the brightest staining of EF5 and pimonidazole were manually selected in Photoshop. The brightness of the top 1% of pixels in

this region was used to define the maximum brightness for the entire section. In effect, this assumes that the brightest pixels in the pimonidazole and EF5 images represent the same level of hypoxia—i.e., complete anoxia; and that all sections contain regions of complete anoxia. In defense of this assumption, the brightest regions for both markers were immediately adjacent to areas of necrosis, where complete anoxia would be expected.

Using the Optipix Wide Histogram plugin (Reindeer Graphics, Ashville NC), the histograms of fluorescent intensity were exported to Excel where they were converted into cumulative form. Images of hypoxia markers are frequently analyzed by applying a threshold, and obtaining the positive fraction defined as the fraction of pixels greater than the threshold. Cumulative histograms show how the positive fraction would change as a function of the threshold. Further, it is possible to calculate the ratio of the fraction staining positive for marker 1 compared to marker 2 for each threshold value. This calculation was performed over the threshold range 30–120. A value of 30 is close to background—i.e., the minimum level of fluorescence found throughout the sections. We consider values beyond 120 irrelevant since a threshold value of 120 treats pixels that are clearly positive (they have a brightness more than twice that of background) as negative for marker. This process was applied to all tumors in each treatment group, so that for every threshold value we obtained the mean ratio. Also for each threshold value, controls and treated groups were compared and a p-value obtained, using a two tailed unpaired t-test.

Correlation of red and green fluorescence intensities for each pixel in the viable tumor area was achieved using in-house software written in Interactive Data Language (RSI Boulder, CO). Processed images from Photoshop were imported into the program, where they were co-registered, and regions of interest drawn to exclude areas of necrosis.

Tumor irradiation

5×10^6 HT29 cells were implanted into the right hind leg of male Balb/c athymic nude mice (Shizuoka Laboratory Center, Hamamatsu, Japan). Experiments were performed when the mean tumor volume was 170 mm^3. Mice were randomly assigned to one of four groups: control; Atrasentan alone; radiation alone; Atrasentan plus radiation. Atrasentan was delivered as above 6 h prior to radiation. Irradiation was delivered using a ^{60}Co., Teletherapy unit (Theratron 780, Atomic Energy of Canada, Chalk River, Canada) to tumor covered with a 5 mm thick tissue equivalence bolus. Tumors received a single dose of 20 Gy at a dose rate of 122.58 cGy/min. Mice were anesthetized with Zoletil/Xylazine prior to irradiation. Each group contained five animals. Two perpendicular diameters of tumors were measured every two days with a digital caliper and tumor volume was calculated according to the following formula: $V\ (mm^3) = \pi/6 \times \text{length} \times \text{width}^2$. Measurement was continued until tumor volume reached at least four times the starting volume. Growth delay—defined as the time to reach four times the starting volume were compared using a 2-tailed Mann-Whitney test (www.quantitativeskills.com/sisa/). All animal protocols and studies were conducted in accordance with the guidelines of the Institutional Animal Care and Use Committee of the Korea Institute of Radiological and Medical Sciences, Korea.

Abbreviations

DCE-MRI	dynamic contrast enhanced magnetic resonance imaging
EF5	2-(2-nitro-1H-imidazol-1-yl)-N-(2,2,3,3,3-pentafluoropropyl)acetamide
ET	endothelin
Gd DTPA	gadolinium diethylenetriaminopentaacetic acid

IR	ionizing radiation

Acknowledgments

This work was funded by NIH-NCI PO1CA115675-A1, R24CA83084 and CA098505. This publication acknowledges Grant Number NCI P30-CA 08748, which provides partial support for the Research Animal Resource Center. K.M.Y. was supported by funds from the Korean Cancer Research Institute.

Atrasentan was supplied by Abbott Laboratories, Chicago, IL.

References

1. Nelson J, Bagnato A, Battistini B, Nisen P. The endothelin axis: emerging role in cancer. Nat Rev Cancer 2003;3:110–116. [PubMed: 12563310]
2. Schneider MP, Boesen EI, Pollock DM. Contrasting actions of endothelin ET(A) and ET(B) receptors in cardiovascular disease. Annu Rev Pharmacol Toxicol 2007;47:731–759. [PubMed: 17002597]
3. Hayasaki Y, Nakajima M, Kitano Y, Iwasaki T, Shimamura T, Iwaki K. ICAM-1 expression on cardiac myocytes and aortic endothelial cells via their specific endothelin receptor subtype. Biochem Biophys Res Commun 1996;229:817–824. [PubMed: 8954978]
4. Kallakuri S, Kreipke CW, Rossi N, Rafols JA, Petrov T. Spatial alterations in endothelin receptor expression are temporally associated with the altered microcirculation after brain trauma. Neurol Res 2007;29:362–368. [PubMed: 17626731]
5. Yokomori H, Oda M, Ogi M, Kamegaya Y, Tsukada N, Nakamura M, Ishii H. Enhanced expression of endothelin receptor subtypes in cirrhotic rat liver. Liver 2001;21:114–122. [PubMed: 11318980]
6. Asham E, Shankar A, Loizidou M, Fredericks S, Miller K, Boulos PB, et al. Increased endothelin-1 in colorectal cancer and reduction of tumour growth by ET(A) receptor antagonism. Br J Cancer 2001;85:1759–1763. [PubMed: 11742499]
7. Donckier JE, Michel L, Van Beneden R, Delos M, Havaux X. Increased expression of endothelin-1 and its mitogenic receptor ET_A in human papillary thyroid carcinoma. Clin Endocrinol (Oxf) 2003;59:354–360. [PubMed: 12919159]
8. Ali H, Loizidou M, Dashwood M, Savage F, Sheard C, Taylor I. Stimulation of colorectal cancer cell line growth by ET-1 and its inhibition by ET(A) antagonists. Gut 2000;47:685–688. [PubMed: 11034585]
9. Berry PA, Zhang YF, Carter ND, Jeffery S, Burchill SA. Decreased wild-type full-length Et-A and -B receptors in neuroblastoma and Ewing sarcoma cells. Med Pediatr Oncol 2001;36:142–146. [PubMed: 11464869]
10. Grant ES, Brown T, Roach A, Williams BC, Habib FK. In vitro expression of endothelin-1 (ET-1) and the ET_A and ET_B ET receptors by the prostatic epithelium and stroma. J Clin Endocrinol Metab 1997;82:508–513. [PubMed: 9024245]
11. Pflug BR, Zheng H, Udan MS, D'Antonio JM, Marshall FF, Brooks JD, Nelson JB. Endothelin-1 promotes cell survival in renal cell carcinoma through the ET(A) receptor. Cancer Lett 2007;246:139–148. [PubMed: 16581180]
12. Nelson JB, Udan MS, Guruli G, Pflug BR. Endothelin-1 inhibits apoptosis in prostate cancer. Neoplasia 2005;7:631–637. [PubMed: 16026642]
13. Wu-Wong JR, Chiou WJ, Wang J. Extracellular signal-regulated kinases are involved in the antiapoptotic effect of endothelin-1. J Pharmacol Exp Ther 2000;293:514–521. [PubMed: 10773023]
14. Del Bufalo D, Di Castro V, Biroccio A, Varmi M, Salani D, Rosano L, et al. Endothelin-1 protects ovarian carcinoma cells against paclitaxel-induced apoptosis: requirement for Akt activation. Mol Pharmacol 2002;61:524–532. [PubMed: 11854432]
15. Panettieri RA Jr, Goldie RG, Rigby PJ, Eszterhas AJ, Hay DW. Endothelin-1-induced potentiation of human airway smooth muscle proliferation: an ET_A receptor-mediated phenomenon. Br J Pharmacol 1996;118:191–197. [PubMed: 8733595]

16. Hafizi S, Allen SP, Goodwin AT, Chester AH, Yacoub MH. Endothelin-1 stimulates proliferation of human coronary smooth muscle cells via the ET(A) receptor and is co-mitogenic with growth factors. Atherosclerosis 1999;146:351–359. [PubMed: 10532691]

17. Armstrong AJ, Creel P, Turnbull J, Moore C, Jaffe TA, Haley S, et al. A phase I-II study of docetaxel and atrasentan in men with castration-resistant metastatic prostate cancer. Clin Cancer Res 2008;14:6270–6276. [PubMed: 18829508]

18. Chiappori AA, Haura E, Rodriguez FA, Boulware D, Kapoor R, Neuger AM, et al. Phase I/II study of atrasentan, an endothelin A receptor antagonist, in combination with paclitaxel and carboplatin as first-line therapy in advanced non-small cell lung cancer. Clin Cancer Res 2008;14:1464–1469. [PubMed: 18316570]

19. Nelson JB, Love W, Chin JL, Saad F, Schulman CC, Sleep DJ, et al. Phase 3, randomized, controlled trial of atrasentan in patients with nonmetastatic, hormone-refractory prostate cancer. Cancer 2008;113:2478–2487. [PubMed: 18785254]

20. Battistini B, Berthiaume N, Kelland NF, Webb DJ, Kohan DE. Profile of past and current clinical trials involving endothelin receptor antagonists: the novel “-sentan” class of drug. Exp Biol Med (Maywood) 2006;231:653–695. [PubMed: 16740981]

21. Martinive P, De Wever J, Bouzin C, Baudelet C, Sonveaux P, Grégoire V, et al. Reversal of temporal and spatial heterogeneities in tumor perfusion identifies the tumor vascular tone as a tunable variable to improve drug delivery. Mol Cancer Ther 2006;5:1620–1627. [PubMed: 16818522]

22. Sonveaux P, Dessy C, Martinive P, Havaux X, Jordan BF, Gallez B, et al. Endothelin-1 is a critical mediator of myogenic tone in tumor arterioles: implications for cancer treatment. Cancer Res 2004;64:3209–3214. [PubMed: 15126361]

23. Overgaard J. Hypoxic radiosensitization: adored and ignored. J Clin Oncol 2007;25:4066–4074. [PubMed: 17827455]

24. Kaanders JH, Bussink J, van der Kogel AJ. ARCON: a novel biology-based approach in radiotherapy. Lancet Oncol 2002;3:728–737. [PubMed: 12473514]

25. Hulshof MC, Rehmann CJ, Booij J, van Royen EA, Bosch DA, Gonzalez Gonzalez D. Lack of perfusion enhancement after administration of nicotin-amide and carbogen in patients with glioblastoma: a 99mTc-HMPAO SPECT study. Radiother Oncol 1998;48:135–142. [PubMed: 9783884]

26. Wu-Wong JR, Dixon DB, Chiou WJ, Sorensen BK, Liu G, Jae HS, et al. Pharmacology of endothelin receptor antagonists ABT-627, ABT-546, A-182086 and A-192621: in vitro studies. Clin Sci (Lond) 2002;103:107–111. [PubMed: 12095412]

27. Bagnato A, Cirilli A, Salani D, Simeone P, Muller A, Nicotra MR, et al. Growth inhibition of cervix carcinoma cells in vivo by endothelin A receptor blockade. Cancer Res 2002;62:6381–6384. [PubMed: 12438219]

28. Banerjee S, Hussain M, Wang Z, Saliganan A, Che M, Bonfil D, et al. In vitro and in vivo molecular evidence for better therapeutic efficacy of ABT-627 and Taxotere combination in prostate cancer. Cancer Res 2007;67:3818–3826. [PubMed: 17440096]

29. Vernerova Z, Kramer HJ, Backer A, Cervenka L, Opocensky M, Huskova Z, et al. Late-onset endothelin receptor blockade in hypertensive heterozygous REN-2 transgenic rats. Vascul Pharmacol 2008;48:165–173. [PubMed: 18372220]

30. Sachidanandam K, Elgebaly MM, Harris AK, Hutchinson JR, Mezzetti EM, Portik-Dobos V, Ergul A. Effect of chronic and selective endothelin receptor antagonism on microvascular function in type 2 diabetes. Am J Physiol Heart Circ Physiol 2008;294:2743–2749.

31. Fryer RM, Rakestraw PA, Banfor PN, Cox BF, Opgenorth TJ, Reinhart GA. Blood pressure regulation by ET_A and ET_B receptors in conscious, telemetry-instrumented mice and role of ET_A in hypertension produced by selective ET_B blockade. Am J Physiol Heart Circ Physiol 2006;290:2554–2559.

32. Evans SM, Judy KD, Dunphy I, Jenkins WT, Hwang WT, Nelson PT, et al. Hypoxia is important in the biology and aggression of human glial brain tumors. Clin Cancer Res 2004;10:8177–8184. [PubMed: 15623592]

33. Kaanders JH, Wijffels KI, Marres HA, Ljungkvist AS, Pop LA, van den Hoogen FJ, et al. Pimonidazole binding and tumor vascularity predict for treatment outcome in head and neck cancer. Cancer Res 2002;62:7066–7074. [PubMed: 12460928]
34. Ljungkvist AS, Bussink J, Rijken PF, Raleigh JA, Denekamp J, Van Der Kogel AJ. Changes in tumor hypoxia measured with a double hypoxic marker technique. Int J Radiat Oncol Biol Phys 2000;48:1529–1538. [PubMed: 11121659]
35. Russell J, Carlin S, Burke SA, Wen B, Yang KM, Ling CC. Immunohistochemical detection of changes in tumor hypoxia. Int J Radiat Oncol Biol Phys 2009;73:1177–1186. [PubMed: 19251089]
36. Opgenorth TJ, Adler AL, Calzadilla SV, Chiou WJ, Dayton BD, Dixon DB, et al. Pharmacological characterization of A-127722: an orally active and highly potent ET_A-selective receptor antagonist. J Pharmacol Exp Ther 1996;276:473–481. [PubMed: 8632312]
37. Verhaar MC, Grahn AY, Van Weerdt AW, Honing ML, Morrison PJ, Yang YP, et al. Pharmacokinetics and pharmacodynamic effects of ABT-627, an oral ET_A selective endothelin antagonist, in humans. Br J Clin Pharmacol 2000;49:562–573. [PubMed: 10848720]
38. Guichard M, Dertinger H, Malaise EP. Radiosensitivity of four human tumor xenografts. Influence of hypoxia and cell-cell contact. Radiat Res 1983;95:602–609. [PubMed: 6611864]
39. Hoffmann U, Brix G, Knopp MV, Hess T, Lorenz WJ. Pharmacokinetic mapping of the breast: a new method for dynamic MR mammography. Magn Reson Med 1995;33:506–514. [PubMed: 7776881]

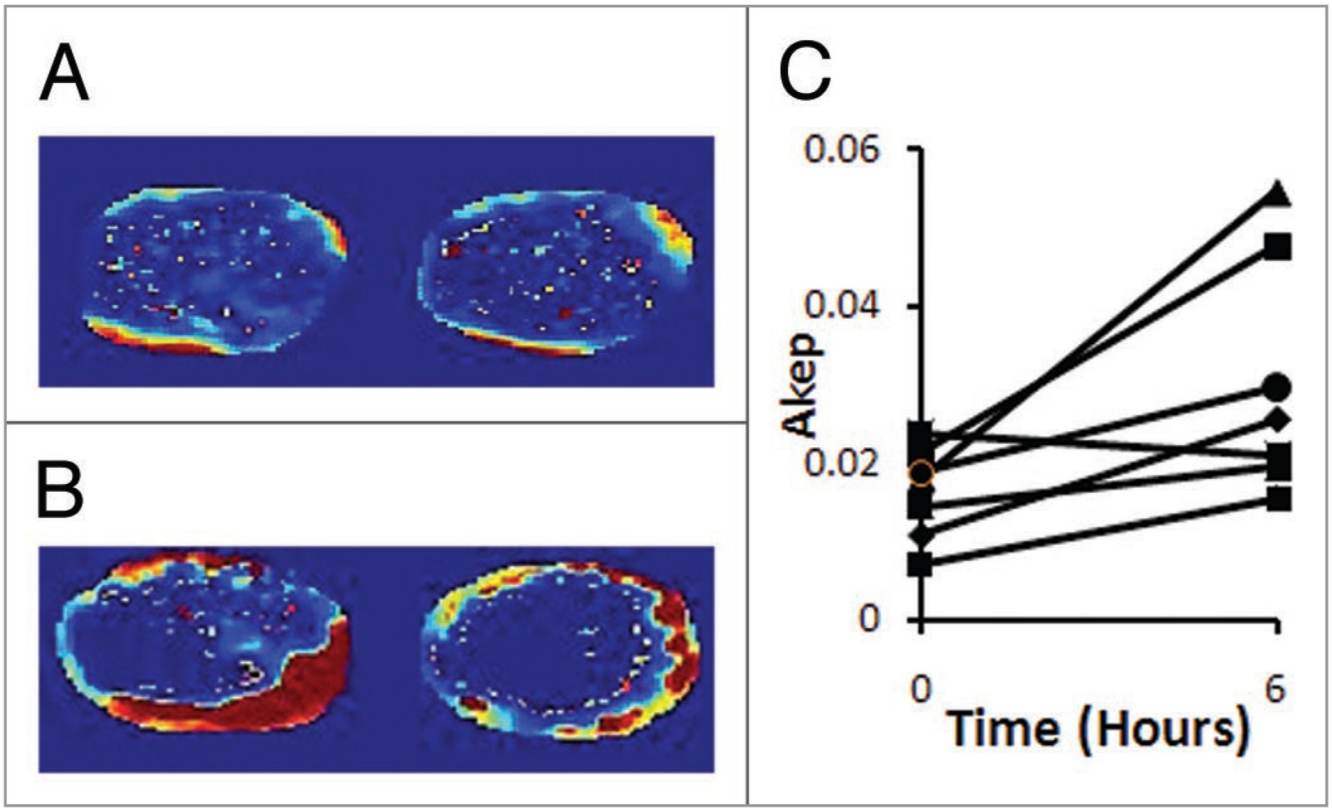

Figure 1.
Tumor perfusion as measured by DCE-MRI. (A) Two slices from a pretreatment tumor. (B) Slices from the same tumor 6 h after Atrasentan administration. (C) Median AK_{ep} values over the course of the experiment.

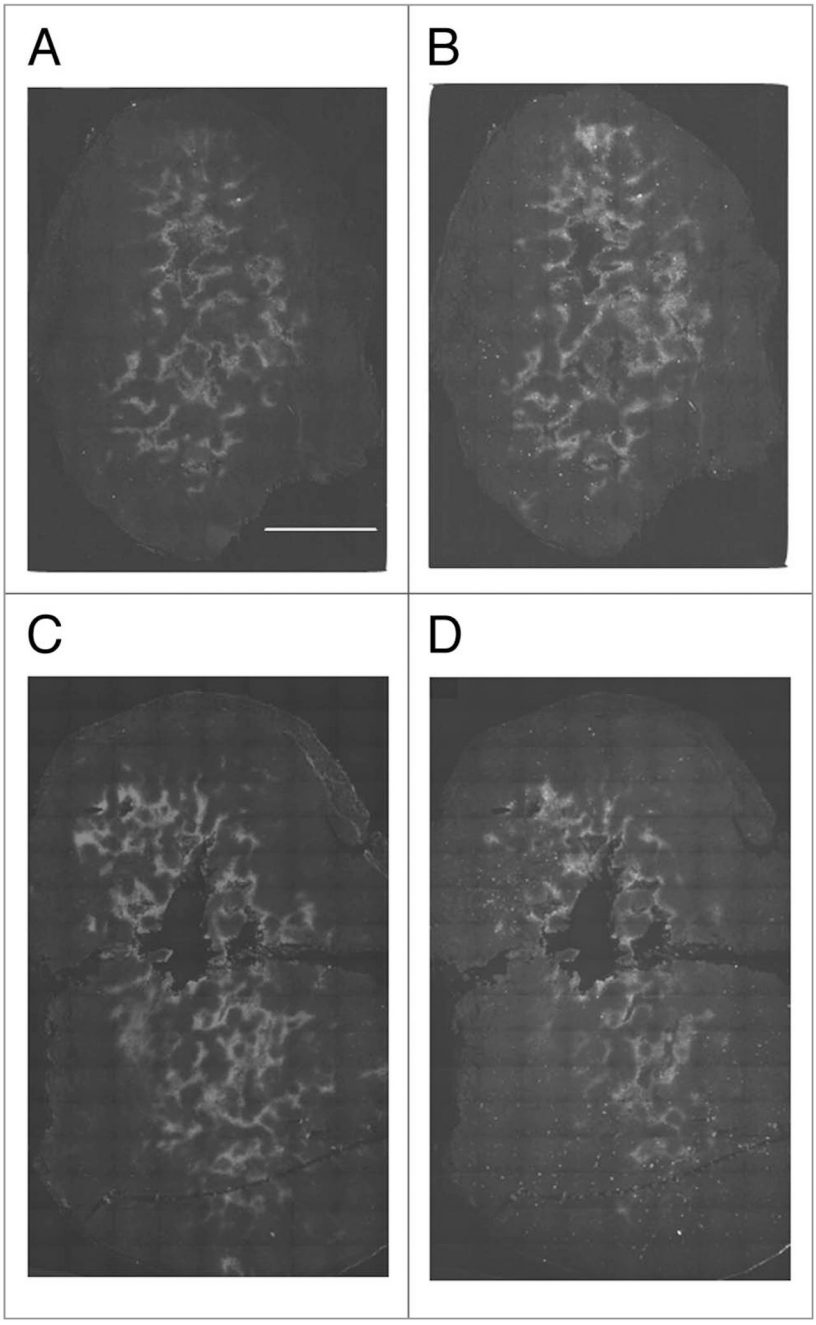

Figure 2.
Changes in tumor hypoxia after Atrasentan administration. (A) Pimonidazole staining in a control tumor. The scale bar equals 2 mm, and all images are on the same scale. (B) The same section stained for EF5. EF5 was administered 24 h after pimonidazole. (C) Pimonidazole staining in a tumor treated with Atrasentan. (D) The same section stained for EF5.

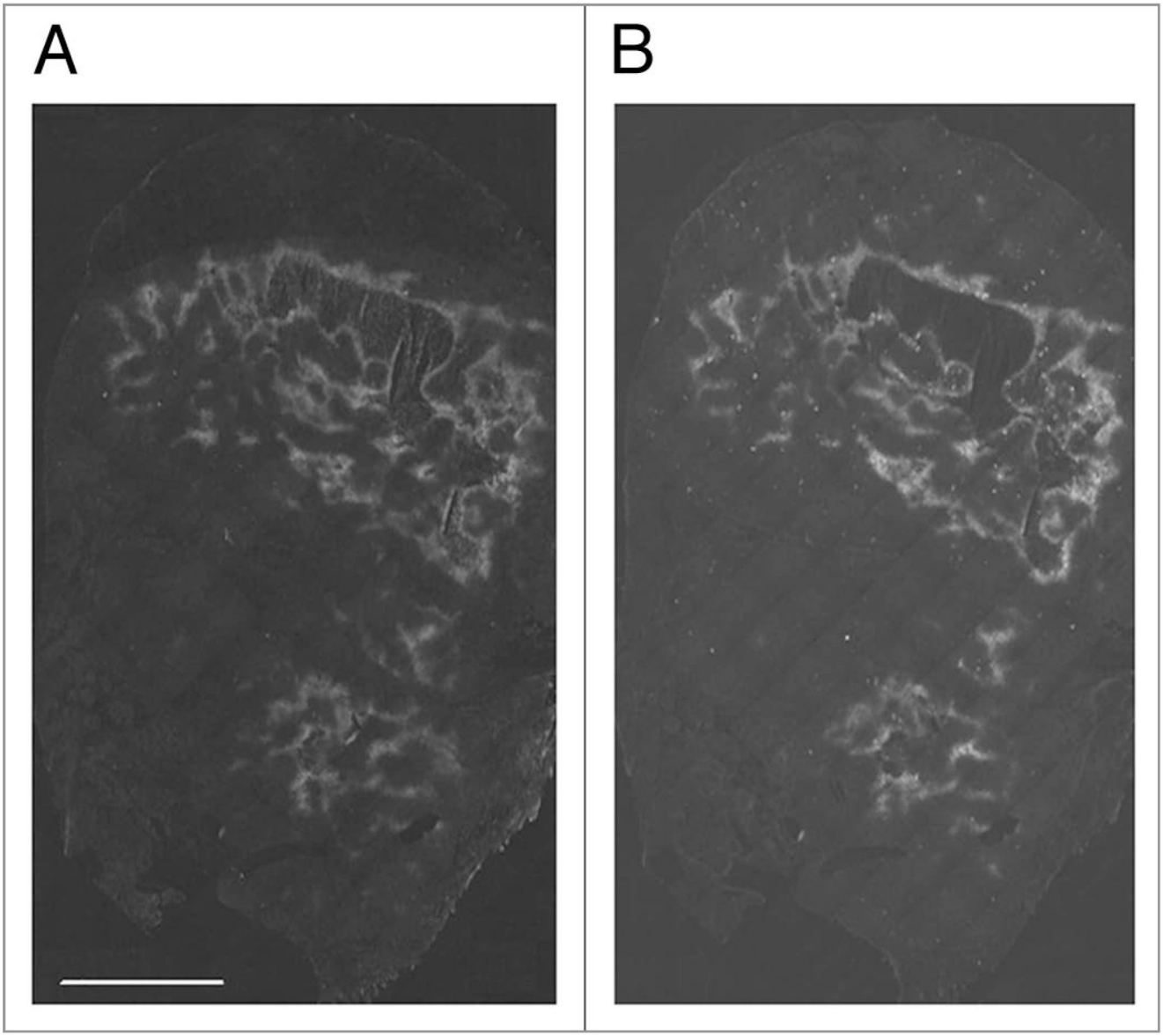

Figure 3.
Tumor hypoxia after Atrasentan administration. (A) Pimonidazole staining in a tumor treated with Atrasentan. (B) The same section stained for EF5.

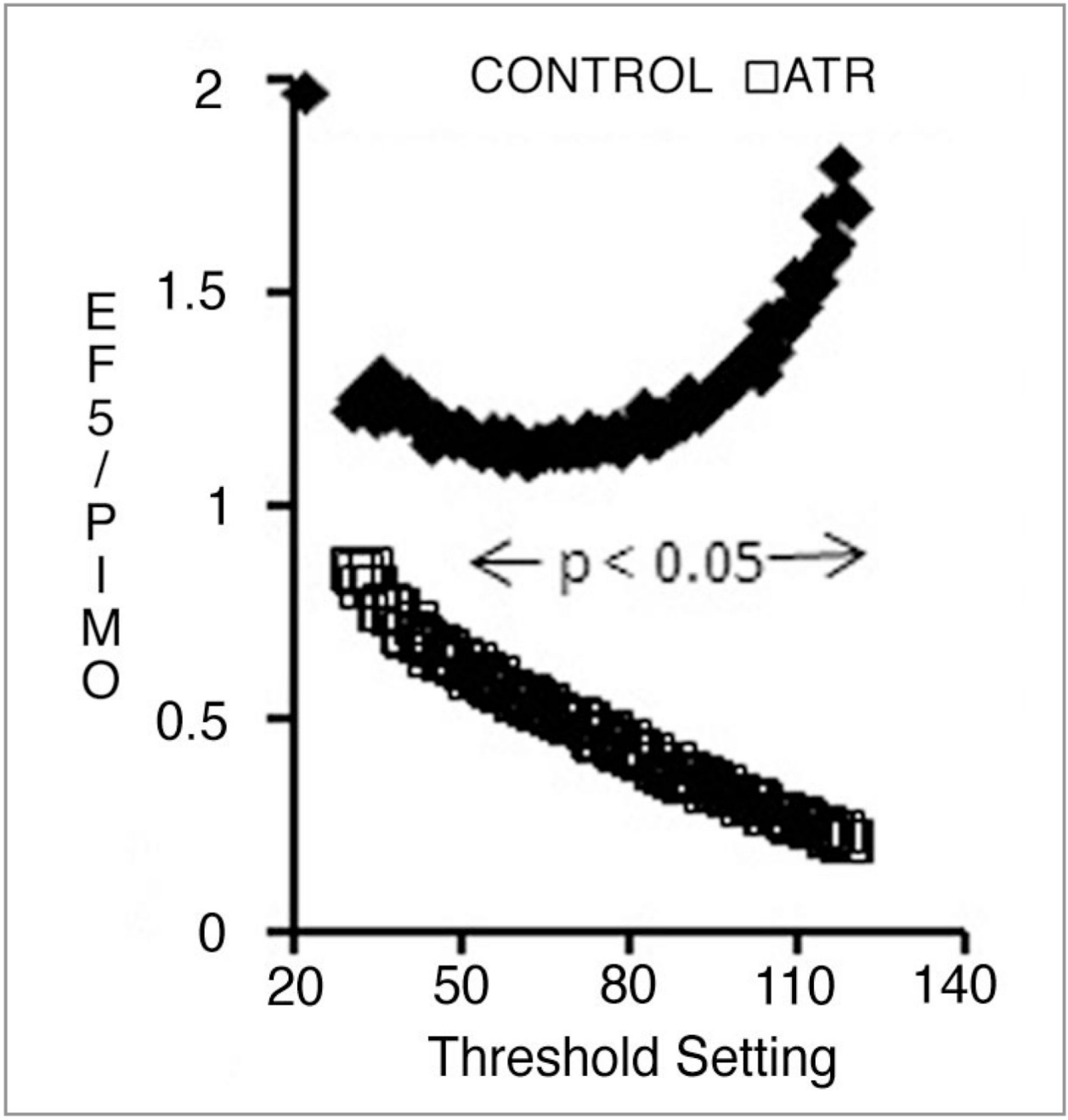

Figure 4.
The fraction of tumor area positive for EF5 relative to the fraction positive for pimonidazole, as a function of threshold setting. Points represent the mean of 4 (control) and 5 (Atrasentan-treated) tumors; the horizontal line shows the range over which a statistically significant difference exists between the two groups.

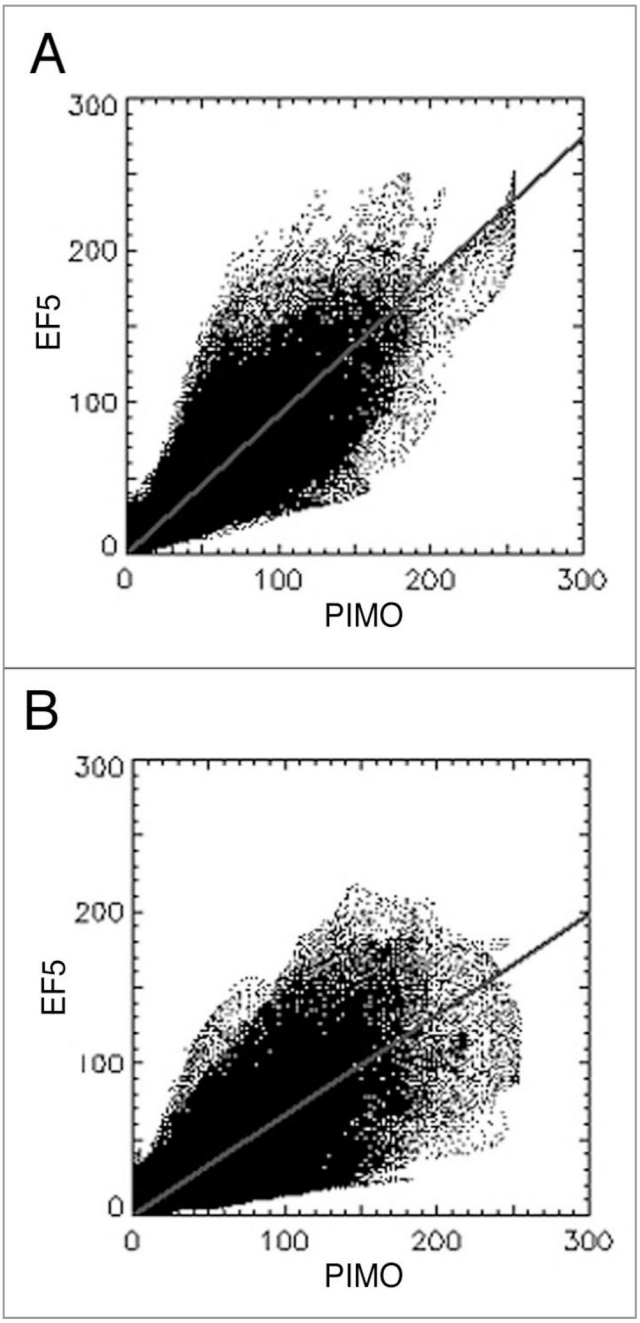

Figure 5.
Representative scatter-plots of EF5 and pimonidazole intensity. (A) control, (B) Atrasentan-treated. Lines represent least squares fit.

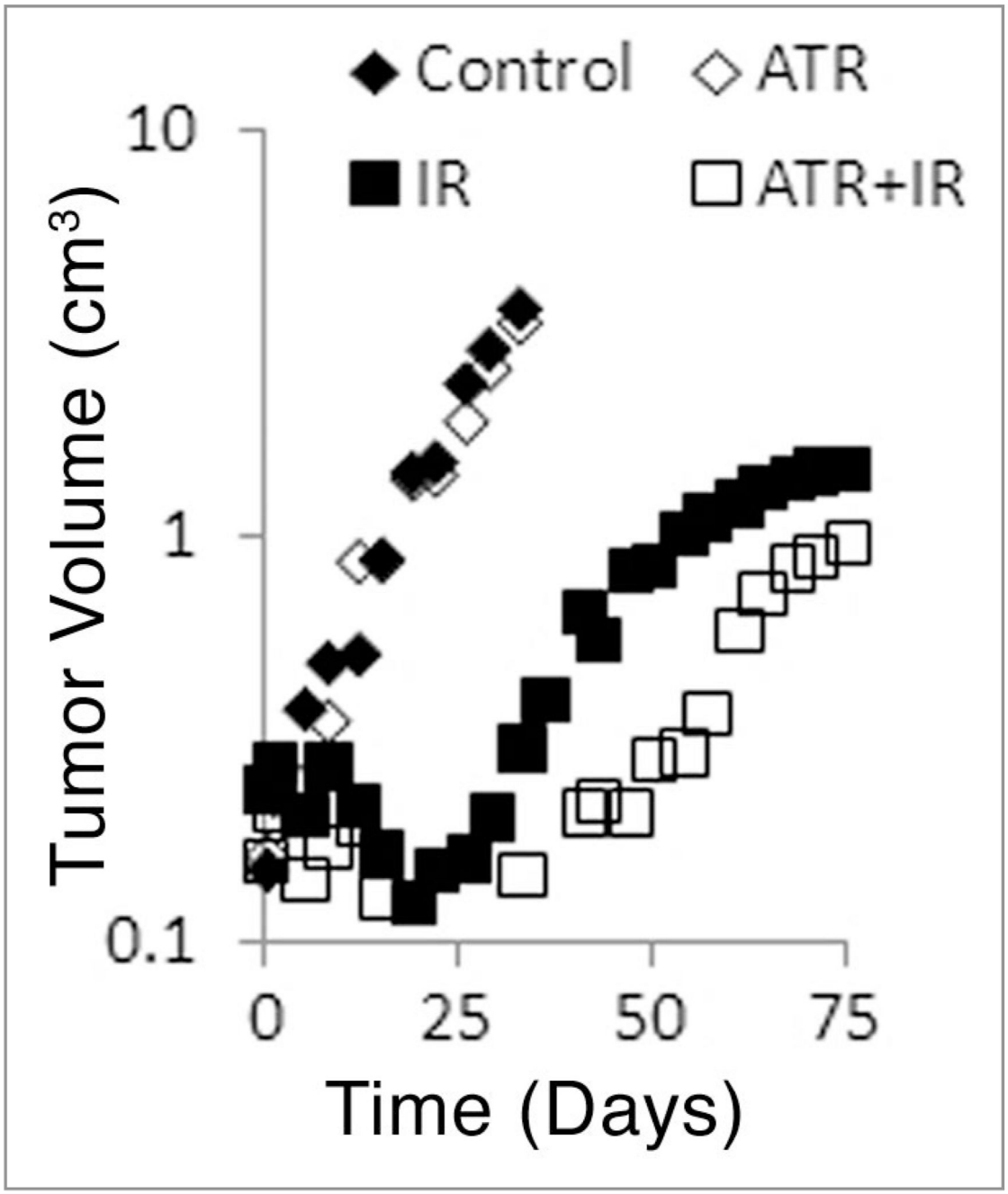

Figure 6.
Regrowth of HT29 tumors. Each point represents the median tumor volume at the specified time. The non-normal distribution of tumor volumes precludes the use of the mean. Tumor volume is plotted on a logarithmic scale.

Table 1

Binary analysis of hypoxia tracer staining

	Percent of section positive for:			
	Pimonidazole	**EF5**	**EF5/PIMO**	**p**
Control	10.8 (4.8–16.8)	11.4 (6.4–16.4)	1.1 (0.7–1.5)	0.012
Atrasentan	9.4 (6.3–12.6)	4.4 (3.5–5.3)	0.5 (0.3–0.7)	

The percent of the tumor section positive was obtained by applying the arbitrarily chosen threshold value of 70 to both markers. Numbers in parentheses represent the 95% confidence range.